



Photonic-assisted high-resolution incoherent back projection synthetic aperture radar imaging

Guanqun Sun, Fangzheng Zhang*, Shilong Pan

Key Laboratory of Radar Imaging and Microwave Photonics, Ministry of Education, Nanjing University of Aeronautics and Astronautics, Nanjing 210016, China

ARTICLE INFO

Keywords:

Microwave photonics
Radar
Back projection algorithm
High-resolution imaging

ABSTRACT

We demonstrate the photonic-assisted high-resolution synthetic aperture radar imaging applying broadband photonic signal generation and a modified incoherent back projection (BP) imaging algorithm. The radar transmits linear frequency modulated (LFM) signals generated by period-one oscillation in an optically injected semiconductor laser. Since the signal bandwidth is greatly enlarged compared with traditional electric radars, a significantly improved imaging resolution can be achieved. Besides, we use a modified incoherent BP imaging algorithm with self-amplitude weighting and multiplicative tomography weighting, to further increase the imaging resolution and to suppress the undesired high-energy artifacts and background interferences. An experiment is carried out. Based on the established radar with a signal bandwidth as large as 12 GHz, high-resolution and clear images of different scenes are successfully constructed, through which the advantages of the proposed scheme over traditional BP imaging system can be soundly verified. The demonstrated scheme provides a good solution to enhance the performance of the incoherent BP imaging algorithm and simultaneously overcome the radar bandwidth limitation. It would find applications where high-resolution radar imaging is needed.

1. Introduction

High-resolution radar imaging plays an important role in many applications such as automatic driving, security check, environmental monitoring and so on [1,2]. Synthetic aperture radar (SAR) is a good solution to improving the imaging resolution by constructing an equivalent large observation aperture. Among the various SAR imaging algorithms, incoherent back projection (BP) algorithm is a common time-domain imaging method that has been widely used in through-the-wall radar, airborne radar, and ground penetrating radar, etc. In an incoherent BP imaging system, by calculating and compensating the round-trip time delay between the radar and target, the echo information is synchronized in time domain and then superimposed layer by layer on the imaging pixels [3,4]. Compared with other SAR imaging methods, incoherent BP algorithm is simple to implement and free from complicated signal processing such as motion compensation [5]. Generally, the image quality of an incoherent BP imaging system is determined by the radar resolution and its capability to suppress the undesired contaminations, such as the high-energy artifacts and the background interferences that are generated when constructing the image layer by layer [6]. Recently, we proposed a modified incoherent BP imaging algorithm with self-amplitude weighting and multiplicative tomography weighting [7]. This method can effectively suppress the undesired high-energy artifacts and background interferences. At the

same time, the imaging resolution can be improved through super-resolution processing, i.e., the self-amplitude weighting. Performance of this method was investigated based on an electrical radar suite having a bandwidth of 3.8 GHz, in which the undesired contaminations were effectively suppressed and the imaging resolution was obviously improved. While, this imaging resolution is still not enough to meet the requirements in many applications such as target recognition. To further improve the imaging resolution, the bandwidth of the radar, which essentially determines the range-resolution, should be further enlarged. This is hard to implement because the bandwidth of current electrical signal generators is usually limited within several GHz [8,9]. Fortunately, the emerging microwave photonic technology provides promising solutions to generating and processing broadband radar signals for radar applications [10–15]. With photonic-assisted radars, coherent inverse SAR (ISAR) imaging with a resolution better than 2 cm has been successfully demonstrated [16–18].

In this paper, we demonstrate the photonic-assisted high-resolution radar imaging with modified incoherent back projection algorithm. This is the first time that the photonic signal generation is introduced to an incoherent BP imaging radar. Specifically, the proposed radar transmits broadband linear frequency modulated (LFM) waveforms generated by period-one (P1) oscillations in semiconductor lasers. Thanks to the use of photonic technologies, the radar bandwidth can easily

* Corresponding author.

E-mail address: zhangfangzheng@nuaa.edu.cn (F. Zhang).

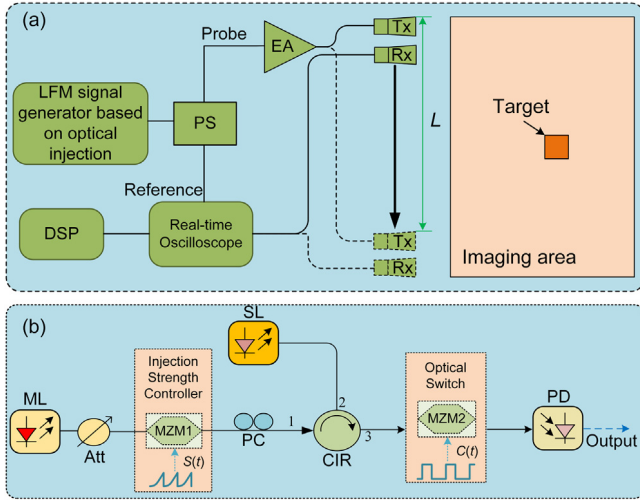


Fig. 1. (a) Schematic diagram of the radar imaging system, (b) Structure of the LFM signal generator. ML: master laser; ATT: optical attenuator; PC: polarization controller; SL: slave laser; PD: photo-detector; CIR: optical circular; MZM: Mach-Zender modulator; PS: power splitter; EA: electrical amplifiers.

go beyond 10 GHz, and the resultant high range resolution detection capability for each radar aperture can greatly enhance the resolution of the final image. In the experiment, a photonics-based radar having a bandwidth as large as 12 GHz is established, based on which high-resolution and clear BP images of different scenes are successfully demonstrated.

2. Principle

Fig. 1(a) shows the schematic diagram of the proposed radar imaging system. The radar transmits a broadband LFM signal generated based on an optically injected semiconductor laser working in the period-one (P1) state [19–21]. The detailed structure of the LFM signal generator is shown in Fig. 1(b), where the master semiconductor laser (ML) provides a continuous wave (CW) light and it is injected to a slave semiconductor laser (SL) through an optical circulator (CIR). The polarization state of the injected light is tuned by a polarization controller (PC) to be aligned with that of the SL, so that a good optical injection efficiency can be ensured. After properly setting the injection strength and the detuning frequency between the ML and the free-running SL, P1 state can be excited [22]. By sending the output signal from the SL to a photodetector (PD) to implement optical-to-electrical conversion, a single-frequency (f_o) microwave signal can be generated. When the detuning frequency is fixed, the P1 oscillation frequency f_o increases almost linearly as the optical injection strength increases. A periodical near-sawtooth electrical signal $S(t)$ is applied to perform intensity modulation of the injection light through a Mach-Zender modulator (MZM1). With this method, a microwave LFM signal can be generated. In this process, the nonlinearity between the output frequency and the injection strength has been compensated by specially designing the electrical control signal $S(t)$ [21]. Thus, the obtained LFM signal would have a good frequency modulation linearity. To transmit pulsed radar signals, a second Mach-Zender modulator (MZM2) is used before the PD to function as a pulse carver, which is realized by driving MZM2 with a two-level electrical signal $C(t)$ to implement on-off keying modulation. Thanks to the widely frequency-tuning property of P1 oscillation, the generated LFM signal can have a very broad bandwidth over 10 GHz. Besides, the bandwidth, center frequency, repetition rate and duty cycle of the generated LFM signal can be tuned by adjusting the parameters of $S(t)$ and $C(t)$. Then, the obtained LFM signal is split into two branches by an electrical power splitter (PS). The signal in one branch is used as the probe, which is amplified by an

electrical amplifier (EA) before emitted to the air through a transmit antenna (Tx). The signal in the other branch is used as a reference. This reference signal and the radar echo collected by a receive antenna (Rx) are captured and digitalized simultaneously by a two-channel analog-to-digital-converter, which is implemented by a multi-channel real-time oscilloscope in our experiment. By changing the position of the antenna pair, a synthetic radar aperture having an enlarged size can be constructed.

The digital signals collected by different sub-apertures are sent to the digital signal processing (DSP) unit. In the digital signal processing (DSP) unit, pulse compression is first performed by simple cross correlation between the reference signal and the echo signal [23]. By doing this, the 1D pulse compression image for the m th sub-aperture ($m = 1, 2, \dots, M$, M is the number of sub-apertures) is obtained, which can be denoted by $R_m(t)$ with t being the round-trip time delay along the range profile. After interpolating the 1D pulse compression image to make it coincide with the image pixels in the desired imaging region [4,5], the 1D coarse image corresponding to the m th sub-aperture is obtained as $R_m(t_{ij})$, where t_{ij} is the round-trip time delay between the m th sub-aperture and the image pixel at the coordinate of (x_i, y_j) . In traditional BP imaging, the coarse images obtained by different sub-apertures are accumulated layer by layer to get the final image. The amplitude at the image pixel (x_i, y_j) is

$$A(x_i, y_j) = \sum_{m=1}^M R_m(t_{ij}) \quad (1)$$

In the image obtained based on Eq. (1), the targets appear in the pixels where the pulse curves of multiple 1D coarse images intersect. In order to increase the quality of the image, we proposed a modified incoherent BP imaging algorithm with self-amplitude weighting and multiplicative tomography weighting [7]. Here, the self-amplitude weighting is to introduce a self-amplitude related weight to the coarse image obtained by each sub-aperture, which achieves super resolution detection by sharpening the peak in the range profile. The output of the image pixel at (x_i, y_j) is given as

$$A(x_i, y_j) = \sum_{m=1}^M [R_m(t_{ij})]^\alpha \quad (2)$$

where α is a positive integer larger than one. This method can effectively improve the coarse image resolution. In Eq. (2), the multiple coarse images are accumulated to get the final image, in which high-energy artifacts and background interferences still exist due to the mutual contamination between different layers. To solve this problem, multiplicative tomography weighting is proposed to construct the final image by

$$A(x_i, y_j) = \prod_{m=1}^M [R_m(t_{ij})]^\alpha \quad (3)$$

In Eq. (3), the amplitudes of the single-layer coarse image to be considered are treated as the weights to the previous cumulated results, i.e., a multiplicative operation is adopted. This way, the artifacts and background interferences can be effectively suppressed, and the target can be clearly distinguished from the non-target area.

It should be noted that, although a large α and/or M is helpful to get a high resolution, the amplitude contrast between different targets may be excessively enlarged. If oversized α and M are used to detect targets with different radar cross sections (RCS), the detected amplitude of targets with smaller RCS will be much less than those with larger RCS. Thus, α and M should be properly chosen to achieve a high resolution while maintaining an acceptable contrast between different targets. This can be implemented though certain amount of attempts based on the imaging results of traditional BP method. On the other hand, the proposed algorithm can be used as a supplementary method to traditional BP algorithm, to distinguish the targets with much higher resolution in a desired area. In addition, this problem can be alleviated by combining the proposed algorithm with other signal processing method, such as the fast BP imaging algorithm [24], in which not all the sub-apertures are used to construct the final image.

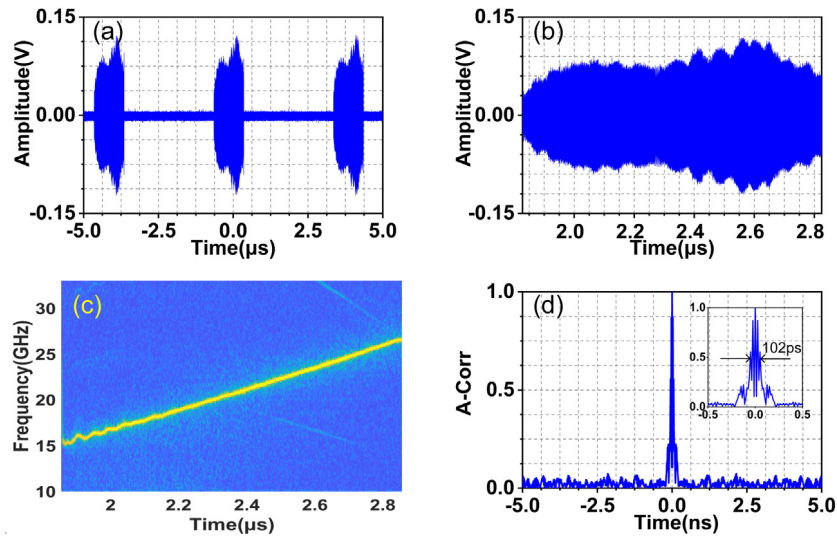


Fig. 2. (a) Measured waveform of the generated LFM signal, (b) the waveform of a single pulse, (c) time–frequency curve corresponding to a periodic waveform (d) autocorrelation results of signal (Insets: the amplified autocorrelation peak).

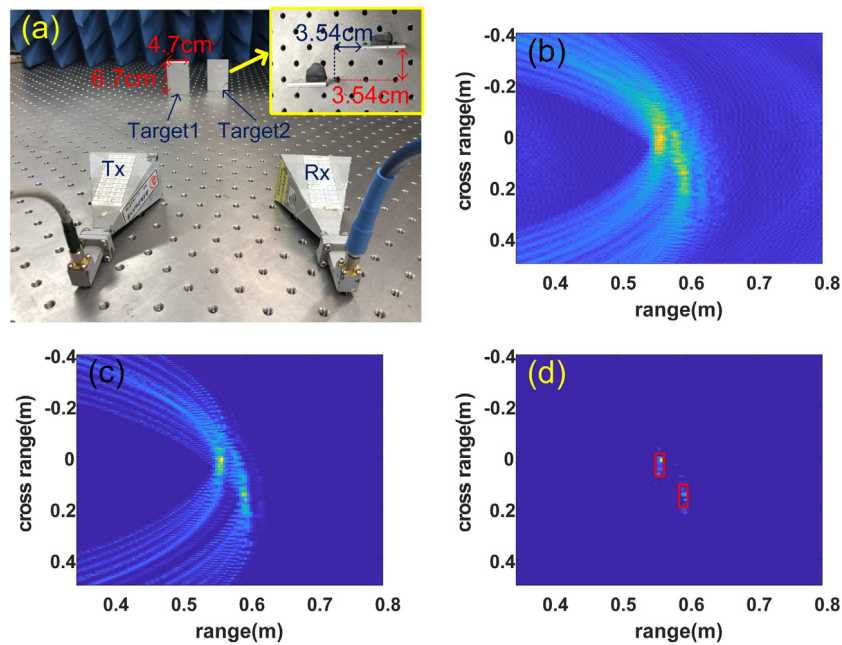


Fig. 3. (a) Photograph of the experimental setup (vertical view of the targets), and the images obtained by (b) traditional BP algorithm, (c) the self-amplitude weighting BP algorithm and (d) self-amplitude weighting combined with multiplicative tomography weighting.

3. Experimental demonstration

A photonics-based radar system is established based on the setup in Fig. 1. The CW light at 1544.012 nm generated by the ML (Agilent N7714A) has a power of 15.8 dBm. The SL is a DFB laser (Actech LD15DM) with a free-running wavelength of 1544.145 nm. It is biased with an electrical current of 32 mA, which is about 5 times of the threshold. The injection strength of the ML is controlled by an MZM (Lucent 2623NA; Bandwidth: 10 GHz), that is driven by a control signal $S(t)$ generated by arbitrary waveform generator (Agilent 81150A; Bandwidth: 120 MHz). The repetition rate of the control signal is 1 MHz. After the SL, another MZM (Lucent 2623NA, Bandwidth: 10 GHz) is followed to implement on–off-keying modulation. The switching signal applied to the second MZM is periodically encoded by “1 0 0 0” with a temporal period of 1 μ s for each bit, and it is synchronized with the control signal $S(t)$. Under proper optical injection, the SL

works in P1 state. By optical-to-electrical conversion through a PD (u2t XPDV2120RA; bandwidth: 40 GHz), a pulsed LFM signal that has a bandwidth of 12 GHz (15–27 GHz) is generated having a duty cycle of 25% and a temporal duration of 1 μ s for each pulse. Fig. 2(a) shows the waveform of the generated LFM signal captured by a real-time oscilloscope (Keysight DSO-X 92504A; Sampling rate: 80 GSa/s). Fig. 2(b) shows the waveform of a single LFM pulse. The corresponding instantaneous frequency recovered by Hilbert transformation is shown in Fig. 2(c). As can be seen, a pulsed LFM signal covering the frequency range of 15–27 GHz is successfully generated. The pulse compression ability of the LFM signal is analyzed by performing autocorrelation with the result shown in Fig. 2(d). In Fig. 2(d), the autocorrelation peak has a full width at half maximum (FWHM) of 102 ps, indicating a pulse compression ratio as high as 9804 is achieved. The generated LFM signal is amplified by an EA (Agilent 83020A) before transmitted to the detection area through a horn antenna. The radar echo is collected

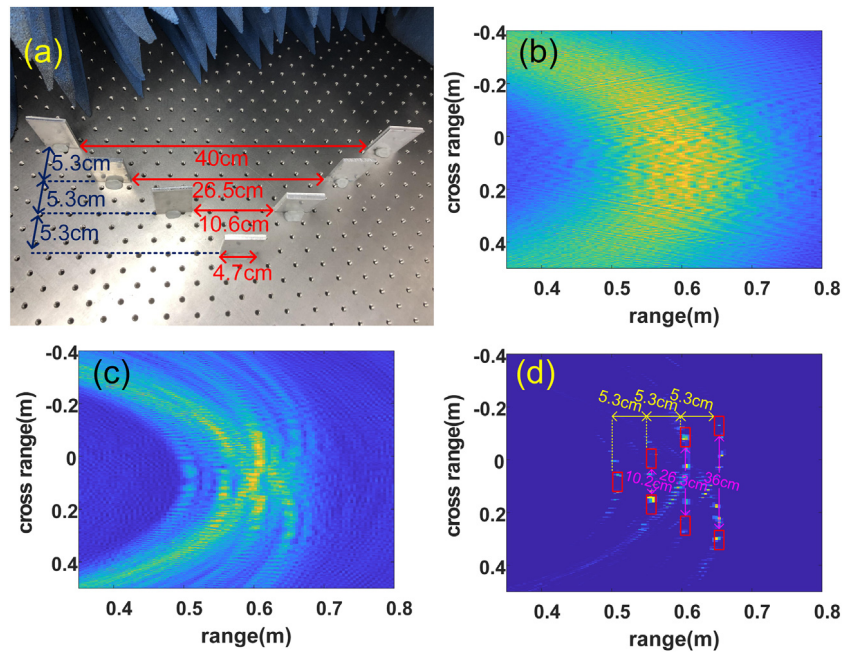


Fig. 4. (a) Close-range photographs of targets, images obtained by experiment with (b) traditional BP algorithm and 1 GHz bandwidth signal, (c) traditional BP algorithm and 12 GHz bandwidth signal, (d) the modified BP algorithm and 12 GHz bandwidth signal.

by another horn antenna and sampled together with the reference LFM signal by two channels of the real-time oscilloscope (Sampling rate: 80 GSa/s for each channel).

To investigate the imaging performance, two metal sheets are used as the target, as shown in Fig. 3(a). In the experiment, positions of the antenna pair are changed to form a uniform linear array with 11 equally spaced apertures having a total length of 35.36 cm. The two metal sheets both have a size of 4.7 cm \times 6.7 cm, and they are separated by 3.54 cm along the range direction. Fig. 3(b) shows the image obtained using traditional BP algorithm, where serious background interferences are observed, making it hard to distinguish the target and the possibility for missed inspection is increased. When self-amplitude weighting algorithm is applied with α being 3 in Eq. (2), the constructed image is shown in Fig. 3(c). As can be seen, the intersecting area of multiple coarse images becomes more focused than the result in Fig. 3(b), because the coarse image resolution is enhanced. While, the artifacts and background interferences due to mutual contamination between different layers still exist. When self-amplitude weighting is applied combined with the multiplicative tomography weighting, the obtained image is shown in Fig. 3(d). In Fig. 3(d), the background interferences and artifacts are removed and the two targets are clearly separated without overlap. This result can verify the advantage of the proposed BP imaging algorithm over the tradition BP imaging algorithm.

Then, radar imaging of a complex target is demonstrated, in which the target consists of 7 metal sheets composing a "V" shaped letter, as shown in Fig. 4(a). In this case, a linear array with 17 equally spaced sub-apertures with a total length of 56.57 cm is adopted. To show the advantage of applying photonics-based broadband LFM signals, radar imaging by transmitting an LFM signal having a bandwidth of 1 GHz, which is comparable with the current electrical signal generators, is performed as a comparison. The 1-GHz bandwidth LFM signal is also generated by the optically injected semiconductor laser and it covers a frequency range of 22.3–23.3 GHz. Fig. 4(b) shows the constructed image with traditional BP algorithm. As can be seen, the low resolution of narrow-band coarse image causes all the small metal sheets to be overlapped in the final image. In addition, there are strong background interferences and artifacts in the image. When the radar transmits LFM signals that have a bandwidth of 12 GHz (15–27 GHz), the image obtained with traditional BP algorithm is shown in Fig. 4(c). Compared

with the image in Fig. 4(b), the resolution is obviously improved, indicating the imaging performance is enhanced by applying photonics-based broadband radar. However, there is still much overlap between different components of the target, and the impact of background interferences and artifacts is still serious. Fig. 4(d) shows the image obtained by the modified BP algorithm with α being 3. As can be seen, the resolution in Fig. 4(d) is much better than those in Fig. 4(b) and (c). In Fig. 4(d), the artifacts and background interferences are well suppressed, and positions of the 7 metal sheets can be clearly distinguished, although slight errors appear in azimuth direction. By increasing the number of sub-apertures to further improve the detection resolution in azimuth direction, more accurate measurement can be guaranteed.

4. Conclusions

We have demonstrated a high-resolution radar imaging system that generates broadband waveforms based on an optically injected semiconductor laser and adopts a modified incoherent BP algorithm to construct the image. Performance of the proposed scheme is investigated through photonics-based radar imaging with a signal bandwidth as large as 12 GHz. The results show that the broad signal bandwidth combined with the proposed BP algorithm achieves much better resolution over traditional BP imaging system and good background suppression. Therefore, the proposed method provides a good solution to overcoming the radar bandwidth limitation and improving the imaging performance.

CRedit authorship contribution statement

Guanqun Sun: Investigation, Writing - original draft, Software. **Fangzheng Zhang:** Conceptualization, Methodology, Writing - review & editing. **Shilong Pan:** Supervision.

Acknowledgments

This work was supported in part by the National Natural Science Foundation of China (61871214), the Natural Science Foundation of Jiangsu Province, China (BK20180066), the Jiangsu Provincial Program for High-level Talents in Six Areas, China (DZXX-005),

the Fundamental Research Funds for the Central Universities, China (NS2018028), and the Foundation of Graduate Innovation Center in NUAA, China (kfjj20190401).

References

- [1] J. Dickmann, N. Appenrodt, H. Bloecher, C. Brenk, T. Hackbarth, M. Hahn, J. Klapstein, M. Muntzinger, A. Sailer, Radar contribution to highly automated driving, in: 2014 44th European Microwave Conference, EuMC, 2014.
- [2] S. Stanko, D. Notel, A. Wahlen, J. Huck, F. Kloppel, R. Sommer, M. Hagelen, Active and passive mmwave imaging for concealed weapon detection and surveillance, in: 2008 33rd International Conference, IEEE IRMMW-THz, 2008.
- [3] L. Carin, N. Geng, M. McClure, J. Sichina, L. Nguyen, Ultra-wideband synthetic aperture radar for mine field detection, in: Ultra- Wideband Short-Pulse Electromagnetics 4 (IEEE Cat. No.98EX112), 1998, pp. 433–441.
- [4] J.I. Halman, K.A. Shubert, G.T. Ruck, SAR processing of ground-penetrating radar data for buried UXO detection: results from a surface-based system, *IEEE Trans. Antennas and Propagation* 46 (7) (1998) 1023–1027.
- [5] L. Zhou, C. Huang, Y. Su, A fast Back-Projection Algorithm based on cross correlation for GPR Imaging, *IEEE Geosci. Remote Sens. Lett.* 9 (2) (2012) 228–232.
- [6] S. Ozsoy, A.A. Ergin, Pencil Back-Projection method for SAR imaging, *IEEE Trans. Image Process.* 18 (3) (2009) 573–581.
- [7] G. Sun, F. Zhang, S. Pan, Improved incoherent Back Projection imaging based on self-amplitude weighting and multiplicative Tomography weighting, in: 2019 IEEE MTT-S International Wireless Symposium, IWS, 2019.
- [8] H. Kwon, B. Kang, Linear frequency modulation of voltage-controlled oscillator using delay-line feedback, *IEEE Microw. Wirel. Compon. Lett.* 15 (6) (2005) 431–433.
- [9] E.D. Adler, E.A. Viveiros, T. Ton, J.L. Kurtz, M.C. Bartlett, Direct digital synthesis applications for radar development, in: Proceedings International Radar Conference, IEEE, 1995, pp. 224–226.
- [10] P. Ghelfi, F. Laghezza, F. Scotti, G. Serafino, A. Capria, S. Pinna, D. Onori, C. Porzi, M. Scaffardi, A. Malacarne, V. Vercesi, E. Lazzeri, F. Berizzi, A. Bogoni, A fully photonics-based coherent radar system, *Nature* 507 (7492) (2014) 341–345.
- [11] R. Li, W. Li, M. Ding, Z. Wen, Y. Li, L. Zhou, S. Yu, T. Xing, B. Gao, Y. Luan, Y. Zhu, P. Guo, Y. Tian, X. Liang, Demonstration of a microwave photonic synthetic aperture radar based on photonic-assisted signal generation and stretch processing, *Opt. Express* 25 (13) (2017) 14334–14340.
- [12] S. Peng, S. Li, X. Xue, X. Xiao, D. Wu, X. Zheng, B. Zhou, High-resolution W-band ISAR imaging system utilizing a logic-operation-based photonic digital-to-analog converter, *Opt. Express* 26 (2) (2018) 1978–1987.
- [13] F. Zhang, B. Gao, S. Pan, Photonics-based MIMO radar with high-resolution and fast detection capability, *Opt. Express* 26 (13) (2018) 17529–17540.
- [14] F. Zhang, Q. Guo, S. Pan, Photonics-based real-time ultra-high-range-resolution radar with broadband signal generation and processing, *Sci. Rep.* 7 (1) (2017) 13848.
- [15] W. Zou, H. Zhang, X. Long, S. Zhang, Y. Cui, J. Chen, All-optical central-frequency-programmable and bandwidth-tailorable radar, *Sci. Rep.* 6 (1) (2016) 19786.
- [16] X. Ye, F. Zhang, Y. Yang, D. Zhu, S. Pan, Photonics-based high-resolution 3D inverse synthetic Aperture Radar imaging, *IEEE Access* 7 (2019) 79503–79509.
- [17] F. Zhang, Q. Guo, Z. Wang, P. Zhou, G. Zhang, J. Sun, S. Pan, Photonics-based broadband radar for high resolution and real-time inverse synthetic aperture imaging, *Opt. Express* 25 (14) (2017) 16274–16281.
- [18] X. Ye, F. Zhang, Y. Yang, S. Pan, Photonics-based radar with balanced 1/Q de-chirping for interference suppressed high-resolution detection and imaging, *Photonics Res.* 7 (3) (2019) 265–272.
- [19] S. Chan, Analysis of an optically injected semiconductor laser for microwave generation, *IEEE J. Quantum Electron.* 46 (3) (2010) 421–428.
- [20] M. Pochet, N.A. Naderi, Y. Li, V. Kovanis, L.F. Lester, Tunable photonic oscillators using optically injected Quantum-Dash Diode Lasers, *IEEE Photonics Technol. Lett.* 22 (11) (2010) 763–765.
- [21] P. Zhou, F. Zhang, Q. Guo, S. Pan, Linearly chirped microwave waveform generation with large time-bandwidth product by optically injected semiconductor laser, *Opt. Express* 24 (16) (2016) 18460–18467.
- [22] P. Zhou, F. Zhang, Q. Guo, S. Li, S. Pan, Reconfigurable Radar Waveform generation based on an optically injected semiconductor laser, *IEEE J. Sel. Top. Quantum Electron.* 23 (6) (2017) 1–9.
- [23] D. Massonnet, J.-C. Souyris, Imaging with synthetic aperture radar, 2008.
- [24] L. Zhang, H. Li, Z. Qiao, M. Xing, Z. Bao, Integrating autofocus techniques with fast factorized back-projection for high-resolution spotlight SAR imaging, *IEEE Geosci. Remote Sens. Lett.* 10 (2013) 1394–1398.